Unsupervised Nuclei Segmentation using Spatial Organization Priors

Loïc Le Bescond, Marvin Lerousseau, Ingrid Garberis, Fabrice André, Stergios Christodoulidis, Hugues Talbot, Maria Vakalopoulou

Unsupervised Nuclei Segmentation using Spatial Organization Priors

Loïc Le Bescond[1,2], Marvin Lerousseau[1], Ingrid Garberis[2], Fabrice André[2], Stergios Christodoulidis[3], Hugues Talbot[1], and Maria Vakalopoulou[3]

[1] Université Paris-Saclay, CentraleSupélec, Centre de Vision Numérique, 91190, Gif-sur-Yvette, France.
[2] Gustave Roussy Cancer Campus, 94800 Villejuif, France.
[3] Université Paris-Saclay, CentraleSupélec, Mathématiques et Informatique pour la Complexité et les Systèmes, 91190, Gif-sur-Yvette, France.

Abstract. In digital pathology, various biomarkers (e.g., KI67, HER2, CD3/CD8) are routinely analysed by pathologists through immunohistochemistry-stained slides. Identifying these biomarkers on patient biopsies allows for a more informed design of their treatment regimen. The diversity and specificity of these types of images make the availability of annotated databases sparse. Consequently, robust and efficient learning-based diagnostic systems are difficult to develop and apply in a clinical setting. Our study builds on the observation that the overall organization and structure of the observed tissues is similar across different staining protocols. In this paper, we propose to leverage both the wide availability of hematoxylin-eosin stained databases and the invariance of tissue organization and structure in order to perform unsupervised nuclei segmentation on immunohistochemistry images. We implement and evaluate a generative adversarial method that relies on high-level nuclei distribution priors through comparison with largely available hematoxylin-eosin stained cell nuclei masks. Our approach shows promising results compared to classic unsupervised and supervised methods, as we demonstrate on two publicly available datasets.

Keywords: Precision medicine · Biomedical imaging · Digital pathology · Generative Adversarial Networks.

1 Introduction

Learning nuclei segmentation models is a challenging problem for immunohistochemistry (IHC) stained histological images. In routine pathology, IHC images are used to provide a distinct readout for proteins at the surface of nuclei or cell membranes that would otherwise be invisible to the human eye, using immunostains [3]. IHC is widely used for diagnostic and for treatment selection, notably in cancer pathology, since it bypasses the need to perform expensive and time-consuming genetic testing. There are over 100 immunostains routinely used by pathologists, highlighting different proteins such as Ki67 and HER2, which can provide clues to tumor proliferation. The segmentation of nuclei stained as such

provides essential information for distinguishing benign cells from malignant cells or those which express a specific protein from those which do not. The ability to automatically identify and segment nuclei in IHC images is crucial since It could *(i)* accelerate the diagnosis time of cancers, *(ii)* reduce misdiagnosis in routine pathology, and *(iii)* improve the performance of cell-based learning system for therapy response prediction.

The most popular nuclei segmentation approaches currently rely on manually obtained, careful pixel-based annotations of nuclei [16,17,26,30]. However, producing such annotations is time-consuming, cumbersome, tedious and error-prone, which hampers the development of segmentation models for a wide range of immunostains. Some semi-supervised methods such as [11] have been proposed to alleviate this need, requiring however manual interactions making their use on whole slide level time consuming. On the other hand, current unsupervised segmentation approaches, such as those based on color clustering, perform inadequately, preventing their application in clinical settings.

This study introduces an approach that revolves around a simple idea: we exploit the fact that the spatial organization and shape characteristics of cells in histological tissue do not change significantly with the type of stain used to color tissue slides. Specifically, we design and evaluate a powerful and highly versatile adversarial-based approach that leverages already publicly available nuclei annotations for haematoxylin-eosin (H&E) stainings to learn segmentation models for potentially many types of immunostains.We show in our experiments that our approach is effective for two of the most prevalent types of nuclear-based and membranous-based immunostains. On these examples, our approach obtains results which are close to fully supervised approaches evaluated on two publicly available datasets, without requiring any annotation.

2 Related Work

Nuclei segmentation is attracting a lot of attention lately with different challenges focusing on methods that can provide accurate segmentations for the many and diverse nuclei present on histology slides [5,32]. These challenges however focus on fully supervised methods, mostly in the domain of H&E stains. Similar approaches relying on manually obtained pixel-based annotations on H&E sometime generalize to some IHC stains e.g., for HER2-stained segmentation [27] and StarDist [29]. However, these methods essentially use color augmentation strategies [18,24], which would be specific to each new staining. In practice, there is a trade-off between the available amount of annotated tiles and the expressive power of the annotations: a higher number of annotated tiles can improve the generalization performance of segmentation systems due to the higher variability of the training data.

Conversely, a variety of thresholding-based approaches have been investigated for unsupervised nuclei segmentation, either based on Otsu thresholding [12,20] or constrained local thresholding [2,19,31]. Self-supervised learning has also been investigated for nuclei segmentation. In [28], authors train a network to accu-

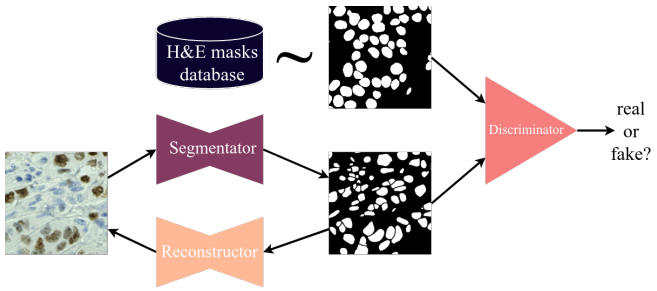

Fig. 1. An overview of our proposed framework.

rately classify the magnification of an input tile using an attention module, and show that the attention maps can be used to produce detection maps of nuclei in H&E staining which can be further converted into nuclei segmentation maps.

Cross-domain learning is a paradigm that consists of the adaptation of a model from one domain to another; for instance from the H&E domain to the IHC domain. In this vein, authors of [13] tackle H&E-IHC cross-domain learning by matching the distribution of high-level features obtained from both domains, for tissue segmentation. Other recent approaches have leveraged the use of generative adversarial networks (GANs) to train segmentation network with various approaches. GANs can be used to generate images via style transfer and use annotations provided in a domain into another, which can then be used to train a supervised network like a U-Net of a Mask-RCNN [13,14]. Moreover, in [33] an auto-encoder like approach for image-to-image translation for style transfer is proposed, learning the segmentation and transfer simultaneously.

Contrary to these approaches, our method exploits the available information at the segmentation level, by encoding and identifying the histological tissue characteristics that are independent of the explored staining. To the best of our knowledge this is the first time that such a scheme is explored, and shown to provide close to fully supervised performance.

3 Methodology

In this study, we propose an unsupervised method for nuclei segmentation incorporating priors from public available datasets. The intuition for our work is that the underlying spatial organization of cells within tissues is the same irrespective of staining. For a given immunostain, rather than relying on specific pixel-based annotations, our approach exploits generic pixel-based segmentation annotations from classical H&E-stained histological images.

Our architecture is composed of three different components trained jointly, as illustrated in Figure 2. The first is a generator (S) which generate segmentation maps from the IHC inputs. The output of S is then processed by a discriminator (D_S) which predicts if the produced segmentation is plausible or not. Moreover, real, unpaired segmentation from public datasets are given to the discriminator,

in order to guide and encode real tissue characteristics. The last component of our method relies in a reconstruction generator (R) which trained to reconstructs IHC-looking nuclei from a segmentation. This way our framework enforces consistency priors between the generated and the real tiles.

Formally, given an input IHC tile t from a training of T, the segmentator S produces a predicted segmentation map $S(t)$. Given a database $\mathcal{DB}$ of segmentation maps from any type of staining (e.g., H&E), a ground-truth segmentation map S_{GT} is sampled from $\mathcal{DB}$ for each IHC tile t. The discriminator D is then asked to correctly predict that each S_{GT} is real (label 1) and that each predicted IHC segmentation map S_{GT} is fake (label 0); this is done by minimizing $\mathcal{L}_D$:

$$\mathcal{L}_D = \big(D(S_{GT}) - 1\big)^2 + \big(D(S(t))\big)^2 \tag{1}$$

Conversely, the segmentator S is optimized by maximizing its ability to fool, i.e. by minimizing the loss function $\mathcal{MSE}_G$ that is:

$$\mathcal{L}_G = \big(D(S(t)) - 1\big)^2 \tag{2}$$

The two examined losses $\mathcal{L}_D$ and $\mathcal{L}_G$ should train S to produce segmentation maps that contain nuclei object that resembles true nuclei segmentation (shape prior), and that display nuclei distribution similar to the nuclei distribution of $\mathcal{DB}$ (organization prior). In fact, with both losses $\mathcal{L}_D$ and $\mathcal{L}_G$ combined, the system is optimized when the distributions of $\mathcal{DB}$ and $\{S(t), t \in T\}$ are matched.

However, we found that the segmentation model S tended to produce false negatives by failing to segment some nuclei. The reconstructor R is intended to circumvent this, by reconstructing the input IHC tile t from its predicted segmentation $S(t)$; nuclei that would be missed by S would then induce errors in the reconstruction $R(S(t))$, therefore inducing S to minimize the number of false negatives. R is trained by minimizing the reconstruction $\mathcal{L}_R$, where an ℓ_1 norm is used for sparsity:

$$\mathcal{L}_R = \big\|R(S(t)) - t\big\|_1 \tag{3}$$

Following CycleGAN [34], we add another discriminator on the IHC and reconstructed IHC domains, in order to train R (and therefore S through backpropagation) with an additional loss beyond pixel-based. For simplicity, we merge this discriminator loss within $\mathcal{L}_D$, and the corresponding adversarial loss of R within $\mathcal{L}_R$ and $\mathcal{L}_G$.

Furthermore, we introduce an additional consistency loss for robustness and to ensure that the segmentator does not solely focus on color for decision making. For an IHC tile t, we consider two color augmentations c_1 and c_2 (e.g. color jitter) and two augmented views $c_1(t)$ and $c_2(t)$ of t. The consistency loss is defined as the ℓ_1 norm between the predicted segmentation maps of both augmented views:

$$\mathcal{L}_C = \big\|S(c_1(t)) - S(c_2(t))\big\|_1 \tag{4}$$

Finally, we sharpen the predicted segmentation maps $S(t)$ by multiplying the predicted logits of the segmentator S using a sharpening factor r=60, similarly

to [7]. This result in saturated value of 0 or 1 rather than float values in $[0, 1]$ which can be used by the discriminator D to easily identify fake segmentations.

The system is trained end-to-end, by optimizing both modules through minimization of the following loss function:

$$\mathcal{L}_{\text{system}} = \mathcal{L}_D + \mathcal{L}_G + \mathcal{L}_R + \mathcal{L}_C \tag{5}$$

4 Experimental Configuration

4.1 Databases

We performed extensive experiments on 3 immunohistochemistry datasets to measure the performance of all benchmarked approaches. In detail, we utilize the **DeepLIIF dataset** [6] with 1667 Ki67-stained fields of view of size 512 pixels at 40x magnification. We used the same data splitting than publicly available, i.e. 709 images for training, 303 for validation and 598 for testing. Immunofluorescence correspondences in the dataset were discarded for the current study. Each image is supplied with ground-truth annotations, which were used for testing purposes but never for our training except for the fully supervised benchmark comparisons. Ki767 IHC images are actually colored with haematoxylin, which marks all nuclei, and Ki67, which marks pKi67 at the surface of some nuclei; nuclei of Ki67-stained images are thus either brown or blue. We also employ he **BCDataset** [8] which consists of 1338 Ki67-stained 640 pixel-width 40x fields of view. Each nucleus is annotated with a single point highlighting its center. These were never used for our training except for testing purposes. Lastly, we use also the **Warwick HER2 dataset** [22,23] which contains 84 HER2-stained whole slide images (WSI) split in 50 training and 34 testing images. We extracted 256x256 patches from each tiles after performing contours detection and filtering based on texture and lightness criteria [15]. To get a good representation of each tissue, we performed K-Means clustering on the Resnet features of each patch and selected for each one the closest to centroids [10]. As KMeans is sensitive to outliers, we applied an isolation forest algorithm to remove the few artifacts that may remain after our pre-processing steps. For the testing set, we divided the patch sets into 2 folds leading to 68 patches. Similarly, for the training set, we divided the patch sets into 14 folds leading to 700 patches. The testing tiles were finally annotated by a expert anatomopathologist.Compared to Ki67, HER2-stained images are more challenging since HER2 marks the membranes of cells (and not their nuclei).

4.2 Baselines

We compare the performance of our proposed method with five competing methods, including two fully supervised approaches. Specifically: a fully supervised model based on **Unet** [9] was utilized. Moreover, **NuClick** [11] was also employed, a weakly supervised approach specifically designed to compute nuclei masks from point annotations at the center of each cell. To train this model,

a senior pathologist manually annotated all nuclei centers in HER2, and such centers were obtained by computing the centroid of each nuclei ground-truth mask for both DeepLIIF and BCDataset datasets. Furthermore, **StarDist** [29] is a supervised method originally trained on H&E images. For our problem, this approach can be considered unsupervised since it does not rely on extra annotations. StarDist was used as a plugin within QuPath [1]. **Thresholding** was performed by applying Otsu thresholding on the Gaussian filtered luminance image. We also applied the same protocol to images obtained through color deconvoluton [25] but this method was found to perform worse. The **proposed** approach was implemented with Unet-styles segmentator S and reconstructor R, and PatchGAN-based discrimators D_R and D_S [9]. At each iteration, a segmentation map $S(t)$ is produced by G for an input IHC tile t. $S(t)$ is forwarded into the discriminator D_S, along with a randomly sampled segmentation map from the Pannuke dataset [4,5] which contains nuclei instance masks of H&E tiles extracted at either 20X or 40X magnification. Similarly, the reconstructor R outputs from these masks simulated IHC images that are compared to the real ones through discriminator D_R. As we found that the reconstruction represents a key factor in the training of our method, we leveraged HER2 membranous nature to train our approach reconstructing only the deconvolved hematoxylin images as nucleus are only highlighted by this marker in this setting [25].

4.3 Implementation Details

We trained the generator using 64 filters in the last convolutional layer and a dropout of 0.5 and Adam optimizer with a learning rate of 0.0002 and $\beta_1 = 0.5$ and $\beta_2 = 0.999$. For the discriminator, we used 64 filters and 3 layers in total, with the same parameters for the optimizer. We exploited nucleus invariance to rotation and flipping to perform data augmentation. Moreover, as our datasets are all extracted from slides scanned at 40X magnifications, we performed random resizing to simulate 20X magnifications images and reproduce Pannuke distribution.

The fully supervised Unet based architecture was tuned on the number of filters $ngf \in [64, 128]$, the dropout value $p \in [0.3 : 0.5]$, the learning rate $lr \in [10^{-5} : 10^{-2}]$, the decay rate $dr \in [10^{-10} : 10^{-3}]$ and the batch size $bs \in [10, 30, 60, 120, 140]$ using a gaussian process algorithm during 50 iterations maximising the F1 score on the validation set after 10 training epochs.

Both fully supervised Unet and the unsupervised proposed approach were then trained on a single A100 GPU for up to 600 epochs with PyTorch v1.10 [21]. For Unet, the model with the lowest validation score was inferred on the (shared) testing set of the DeepLIIF dataset (and was not trained on both other datasets because of missing ground-truth training data). For proposed, the final model was selected by finding the minimum of the system loss $\mathcal{L}_{\text{system}}$ after 250 epochs to discard early training instabilities. To extract nucleus on our method, we first applied a median filter with a window size of 5 to remove the noise that may remain on our final predictions. For HER2 images, we applied in addition an

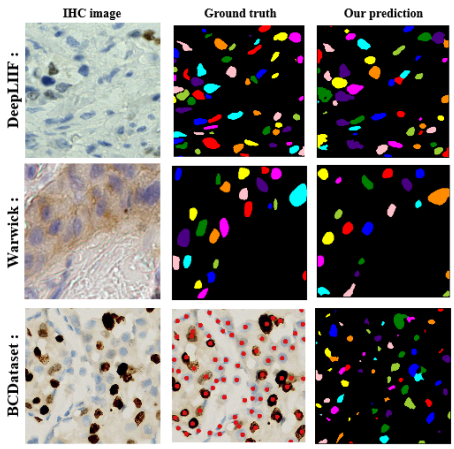

Fig. 2. Examples of predictions of our approach on the different datasets

erosion operation with a radius of 5 to remove remaining artifacts. We lastly applied a watershed algorithm to retrieve final instances [28].

5 Results & Discussion

		Semantic				Object		
Method	Unsupervised	Dice	Accuracy	Precision	Recall	AJI	Dice	Hausdorff
Unet	✗	**77.56**	**84.49**	81.59	**73.95**	40.02	64.30	5.10
Nuclick	✗	76.19	82.57	**86.12**	68.36	**56.70**	**73.18**	**4.76**
Threshold	✓	64.74	75.59	76.68	56.24	29.88	51.66	5.80
StarDist	✓	62.06	73.03	**88.16**	47.95	40.80	52.06	**5.21**
Proposed	✓	**70.27**	**79.86**	74.55	**66.60**	**41.91**	**54.43**	5.77

Table 1. Results on the DeepLIIF dataset [6]. Accuracy is balanced. **Bold** indicates the top performing method for each metric, for both supervised and unsupervised groups.

Table 1 reports semantic and object-level results on the DeepLIIF dataset for Ki67-stained images. The proposed approach obtained the highest Dice score of 70.27 and the highest balanced accuracy of 79.86 among all unsupervised approaches, i.e. approaches that do not necessitate additional annotations. While StarDist [29] obtained a higher precision, the proposed obtained the best recall of unsupervised approaches with 66.60; trading recall for precision is better for clinical considerations as false negative could aggravate the course of the patient care, while false positive can be more easily corrected. The proposed approach obtained competitive results with the fully supervised Unet and the

weakly supervised NuClick which obtained no more than 6% of improvement on the balanced accuracy without requiring any further annotations.

		Semantic				Object		
Method	Unsupervised	Dice	Accuracy	Precision	Recall	AJI	Dice	Hausdorff
Unet	✗	NA	NA	NA	NA	NA	NA	NA
Nuclick	✗	44.55	71.81	40.10	50.46	38.95	56.40	5.21
Threshold	✓	39.85	63.57	64.40	29.05	17.71	39.85	5.59
StarDist	✓	56.85	71.83	**77.86**	44.94	34.81	57.73	**4.29**
Proposed	✓	**62.59**	**77.05**	70.67	**56.51**	**39.29**	**60.01**	4.68

Table 2. Results on the Warwick dataset [22,23]. Accuracy is balanced. **Bold** indicates the top performing method for each metric, for both supervised and unsupervised groups. Unet results are not available (NA) since ground-truth segmentation maps were unavailable.

The Table 2 outlines the results on the testing set extracted from Warwick dataset. Our approach outperforms the other methods on almost all metrics, showing great improvements in semantic metrics with a Dice score of 62.59 and a recall of 56.51 while the classic methods top at 56.85 and 50.46 respectively. Once again, our approach proved to be better tailored to a clinical use with a higher recall and better object metrics. It is also advocating for a great adaptability of our method to the diversity of IHC staining. Indeed, providing minor changes in the training and post-processing, we successfully applied our method to two different staining conditions, thus underlying that our method can better leverage H&E information than directly applying pre-trained state-of-the-art algorithms.

Finally, we assessed the generalisation of the proposed approach trained on DeepLIIF to BCDataset dataset. As highlighted in Fig.2, our approach managed to provide a segmentation matching many ground truth annotations without adding any additional knowledge.

We performed an ablation study that can be found in the supplementary material by successively removing some key components of our method and computing the performances on both DeepLIIF (Ki67 staining) and Warwick (HER2 staining). On both dataset, removing the cycle loss decreased the performances significantly on all the metrics, and produced masks uncorrelated to the input, thus underlying the key role of the proposed cycling architecture. For the consistency loss and the sharpening factor, we noticed that these two elements balanced each other, with a stronger precision but a lower recall when decreasing the sharpening factor, and inversely when removing the consistency loss.

6 Conclusion

In this paper, we introduced a simple yet effective and unsupervised framework for nuclei segmentation integrating spatial organization priors. Extensive exper-

iments on 3 highly heterogeneous datasets highlight the potential of this approach. In particular, we found that our approach outperformed all other benchmarked unsupervised methods as well as some weakly supervised approaches.

There are several axes of improvements over this work. First, besides the nuclei segmentation and detection information, the type of nuclei is also an important information in routine pathology. The current formulation could integrate such information by outputting one segmentation mask per stain and counterstain of IHC images (e.g. HER2 and haematoxylin). Another very interesting direction include the integration of additional datasets or segmentation masks, which would unravel further shape and organization priors for the nuclei.

References

1. Bankhead, P., Loughrey, M.B., Fernández, J.A., et al.: Qupath: Open source software for digital pathology image analysis. Scientific reports **7**(1), 1–7 (2017)
2. Di Cataldo, S., Ficarra, E., Acquaviva, A., Macii, E.: Automated segmentation of tissue images for computerized ihc analysis. Computer methods and programs in biomedicine **100**(1), 1–15 (2010)
3. Duraiyan, J., Govindarajan, R., Kaliyappan, K., Palanisamy, M.: Applications of immunohistochemistry. Journal of pharmacy & bioallied sciences **4**(Suppl 2), S307 (2012)
4. Gamper, J., Alemi Koohbanani, N., Benet, K., et al.: Pannuke: an open pan-cancer histology dataset for nuclei instance segmentation and classification. In: European Congress on Digital Pathology. pp. 11–19. Springer (2019)
5. Gamper, J., Koohbanani, N.A., Benes, K., et al.: Pannuke dataset extension, insights and baselines. arXiv preprint arXiv:2003.10778 (2020)
6. Ghahremani, P., Li, Y., Kaufman, A., et al.: Deep learning-inferred multiplex immunofluorescence for ihc image quantification. bioRxiv (2021)
7. Hou, L., Nguyen, V., Kanevsky, A.B., et al.: Sparse autoencoder for unsupervised nucleus detection and representation in histopathology images. Pattern recognition **86**, 188–200 (2019)
8. Huang, Z., Ding, Y., Song, G., et al.: Bcdata: A large-scale dataset and benchmark for cell detection and counting. In: Medical Image Computing and Computer Assisted Intervention – MICCAI 2020. pp. 289–298. Springer International Publishing, Cham (2020)
9. Isola, P., Zhu, J., Zhou, T., Efros, A.A.: Image-to-image translation with conditional adversarial networks. In: 2017 IEEE Conference on Computer Vision and Pattern Recognition (CVPR). pp. 5967–5976. IEEE Computer Society, Los Alamitos, CA, USA (jul 2017)
10. Kalra, S., Tizhoosh, H., Choi, C., et al.: Yottixel – an image search engine for large archives of histopathology whole slide images. Medical Image Analysis **65**, 101757 (2020)
11. Koohbanani, N., Jahanifar, M., Tajadin, N.Z., Rajpoot, N.: Nuclick: a deep learning framework for interactive segmentation of microscopic images. Medical Image Analysis **65**, 101771 (2020)
12. Kuok, C.P., Wu, P.T., Jou, I.M., et al.: Automatic segmentation and classification of tendon nuclei from ihc stained images. In: Seventh International Conference on Graphic and Image Processing (ICGIP 2015). vol. 9817, p. 98170J. International Society for Optics and Photonics (2015)
13. Lin, Z., Li, J., Yao, Q., et al.: Adversarial learning with data selection for cross-domain histopathological breast cancer segmentation. Multimedia Tools and Applications pp. 1–20 (2022)
14. Liu, D., Zhang, D., Song, Y., et al.: Unsupervised instance segmentation in microscopy images via panoptic domain adaptation and task re-weighting. In: Proceedings of the IEEE/CVF conference on computer vision and pattern recognition. pp. 4243–4252 (2020)
15. Lu, M.Y., Williamson, D.F., Chen, T.Y., et al.: Data-efficient and weakly supervised computational pathology on whole-slide images. Nature Biomedical Engineering **5**(6), 555–570 (2021)
16. Mahanta, L.B., Hussain, E., Das, N., et al.: Ihc-net: A fully convolutional neural network for automated nuclear segmentation and ensemble classification for allred scoring in breast pathology. Applied Soft Computing **103**, 107136 (2021)

17. Mao, K.Z., Zhao, P., Tan, P.H.: Supervised learning-based cell image segmentation for p53 immunohistochemistry. IEEE Transactions on Biomedical Engineering **53**(6), 1153–1163 (2006)
18. Mi, H., Bivalacqua, T.J., Kates, M., et al.: Predictive models of response to neoadjuvant chemotherapy in muscle-invasive bladder cancer using nuclear morphology and tissue architecture. Cell Reports Medicine **2**(9), 100382 (2021)
19. Mouelhi, A., Rmili, H., Ali, J.B., et al.: Fast unsupervised nuclear segmentation and classification scheme for automatic allred cancer scoring in immunohistochemical breast tissue images. Computer methods and programs in biomedicine **165**, 37–51 (2018)
20. Otsu, N.: A threshold selection method from gray-level histograms. IEEE transactions on systems, man, and cybernetics **9**(1), 62–66 (1979)
21. Paszke, A., Gross, S., Massa, F., et al.: Pytorch: An imperative style, high-performance deep learning library. Advances in neural information processing systems **32** (2019)
22. Qaiser, T., Mukherjee, A., Reddy PB, C., et al.: Her2 challenge contest: a detailed assessment of automated her2 scoring algorithms in whole slide images of breast cancer tissues. Histopathology **72**(2), 227–238 (2018)
23. Qaiser, T., Rajpoot, N.M.: Learning where to see: A novel attention model for automated immunohistochemical scoring. IEEE Transactions on Medical Imaging **38**(11), 2620–2631 (2019)
24. Rassamegevanon, T., Feindt, L., Müller, J., et al.: Molecular response to combined molecular-and external radiotherapy in head and neck squamous cell carcinoma (hnscc). Cancers **13**(22), 5595 (2021)
25. Ruifrok, A.C., Johnston, D.A.: Quantification of histochemical staining by color deconvolution. Analytical and quantitative cytology and histology **23**(4), 291–299 (2001)
26. Saha, M., Arun, I., Ahmed, R., et al.: Hscorenet: A deep network for estrogen and progesterone scoring using breast ihc images. Pattern Recognition **102**, 107200 (2020)
27. Saha, M., Chakraborty, C.: Her2net: A deep framework for semantic segmentation and classification of cell membranes and nuclei in breast cancer evaluation. IEEE Transactions on Image Processing **27**(5), 2189–2200 (2018)
28. Sahasrabudhe, M., Christodoulidis, S., Salgado, R., et al.: Self-supervised nuclei segmentation in histopathological images using attention. In: International Conference on Medical Image Computing and Computer-Assisted Intervention. pp. 393–402. Springer (2020)
29. Schmidt, U., Weigert, M., Broaddus, C., Myers, G.: Cell detection with star-convex polygons. In: International Conference on Medical Image Computing and Computer-Assisted Intervention. pp. 265–273. Springer (2018)
30. Sheikhzadeh, F., Ward, R.K., van Niekerk, D., Guillaud, M.: Automatic labeling of molecular biomarkers of immunohistochemistry images using fully convolutional networks. PLoS One **13**(1), e0190783 (2018)
31. Shu, J., Liu, J., Zhang, Y., et al.: Marker controlled superpixel nuclei segmentation and automatic counting on immunohistochemistry staining images. Bioinformatics **36**(10), 3225–3233 (2020)
32. Verma, R., Kumar, N., Patil, A., et al.: Monusac2020: A multi-organ nuclei segmentation and classification challenge. IEEE Transactions on Medical Imaging **40**(12), 3413–3423 (2021)

33. Yao, K., Huang, K., Sun, J., Jude, C.: AD-GAN: End-to-end unsupervised nuclei segmentation with aligned disentangling training. arXiv preprint arXiv:2107.11022 (2021)
34. Zhu, J.Y., Park, T., Isola, P., Efros, A.A.: Unpaired image-to-image translation using cycle-consistent adversarial networks. In: Proceedings of the IEEE international conference on computer vision. pp. 2223–2232 (2017)